Correcting for Beam Spread in Acoustic Doppler Current Profiler Measurements

R. F. MARSDEN

Physics Department, Royal Military College of Canada, Kingston, Ontario, Canada

R. G. INGRAM

Department of Earth and Ocean Sciences, University of British Columbia, Vancouver, British Columbia, Canada

31 October 2002 and 3 March 2004

ABSTRACT

Spatial homogeneity assumptions inherent in the conversion of directly measured acoustic Doppler current profiler (ADCP) beam to Cartesian coordinates for the Janus configuration are investigated. These assumptions may be adequate for large-scale flows, such as tidal currents and wind-forced upwelling. However, for high-frequency features, such as internal solitons and turbulence, the velocity fields may vary over scales comparable to the divergence of the acoustic beams. Equations are derived for beam spreading, and it is shown that a first-order correction can be applied to improve velocity measurement accuracy. Two cases are examined. First, the effects of the spatial and temporal convolution inherent in beam spreading from the Janus configuration ADCP are applied to a model internal solitary wave. It is shown that the corrected vertical velocities have deviations of less than 2 mm s^{-1} for distances up to 30 m from the transducer face and are approximately 3 times more accurate than the uncorrected velocities for distance up to 20 m from the transducer face. Next, under a ''frozen turbulence'' hypothesis, the method is applied to processing turbulence data. It is demonstrated that the horizontal longitudinal velocity can be markedly improved.

1. Introduction

The acoustic Doppler current profiler (ADCP) has taken an increasingly important role in the measurement of both first-order (mean) and second-order (eddy correlation) current statistics. First-order statistics have been used to identify both larger-scale barotropic and baroclinic tidal (Foreman and Freeland 1991; Marsden and Greenwood 1994) and mean flows. At second order, van Haren et al. (1994) and Stacey et al. (1999) have estimated vertical profiles of eddy correlations. Marsden et al. (1994a,b) mounted a narrowband instrument through land-fast ice in the Canadian Arctic and detected numerous instances of apparently significant vertical velocities. Marsden et al. (1995) exploited these vertical velocities to propose a technique for determining internal wave directional spectra. In both instances, the ensemble-averaged velocities were assumed to accurately represent the flow. Problems may arise, however, when measuring first-order small-scale phenomena such as internal waves, solitons, and turbulence.

Corresponding author address: Dr. Richard F. Marsden, Physics Dept., Royal Military College of Canada, P.O. Box 17000 Station Forces, Kingston, ON K7K 7B4, Canada.
E-mail: marsden-r@rmc.ca

The ADCP has either three or four transducers mounted in a symmetric configuration at predetermined angles (typically 20° or 30°) about the vertical (see Fig. 1). It measures a velocity profile by emitting one or more acoustic pulses. The return echo is range gated, and the Doppler shift of the radial velocity is determined in each bin. Of particular interest, for this paper, is the ''Janus'' configuration, whereby four transducers are oriented in vertical planes aligned at 90° between adjacent beams. Lohrmann et al. (1990) have proposed a novel technique for estimating turbulence parameters (specifically Reynolds stress) using this beam orientation. Because of the diverging beams, however, assumptions must be made about the flow statistics to convert from radial to Cartesian velocities. First, the beams measure a spatial average that is rotated relative to the vertical, as is indicated in Fig. 1. Consequently, a portion of the beams overlap adjacent depth cells. RD Instruments (RDI 1996, p. 16) indicates a correction for this effect. More importantly, however, opposing transducers sample different portions of the water column, indicated by the distance $2d \tan\theta$ in Fig. 1. If the length scale of the feature is the same as the beam spread, then velocity errors can occur.

In this note an approach will be presented to correct

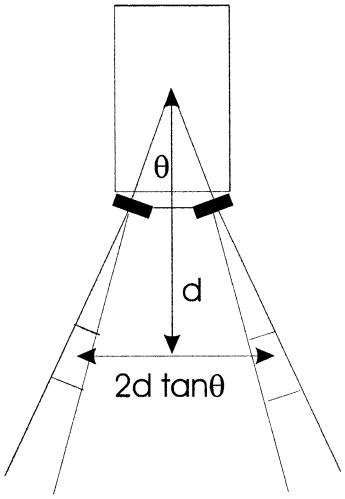

FIG. 1. Schematic of the ADCP beams showing the variables defined in the text.

velocities for beam spread. The correction is based only on the geometry of the Janus configuration and is independent of ADCP manufacturer. The note will be organized in the following manner. Section 2 will present a synopsis and analysis of the inherent convolutions in the data. In section 3, simulations for internal waves and turbulence measurements will be presented. Discussion and conclusions will appear in section 4.

2. Sampling theory and data

Sampling theory

The radial velocities (b_1, b_2, b_3, b_4) for a four-beam downward-looking convex head in the Janus configuration (Fig. 1) actually measure the following Cartesian velocities:

$$b_1(x_0, y_0, z_i) = u[x_0 - s(d_i), y_0, z_i] \sin\theta + w[x_0 - s(d_i), y_0, z_i] \cos\theta, \quad (1a)$$

$$b_2(x_0, y_0, z_i) = -u[x_0 + s(d_i), y_0, z_i] \sin\theta + w[x_0 + s(d_i), y_0, z_i] \cos\theta, \quad (1b)$$

$$b_4(x_0, y_0, z_i) = v[x_0, y_0 - s(d_i), z_i] \sin\theta + w[x_0, y_0 - s(d_i), z_i] \cos\theta, \quad (1c)$$

$$b_3(x_0, y_0, z_i) = -v[x_0, y_0 + s(d_i), z_i] \sin\theta + w[x_0, y_0 + s(d_i), z_i] \cos\theta, \quad (1d)$$

where x_0 and y_0 represent the nominal horizontal position of the transducer and z_i is the nominal depth for the ith cell; $b_j(x_0, y_0, z_i)$ represents a beam velocity, positive toward the transducer $j = 1$–4; u, v, and w are the Cartesian east, north, and vertical velocities, respectively; θ is the deviation of the axis of the beam from vertical; and $s(d_i) = d_i \tan\theta$ is half the horizontal beam separation at a depth cell a vertical distance d_i from the transducer face (see Fig. 1). A little algebra isolates the Cartesian velocities in a more convenient form:

$$\frac{b_1 - b_2}{2\sin\theta} = \frac{1}{2}\{u[x_0 - s(d_i), y_0, z_i] + u[x_0 + s(d_i), y_0, z_i]\} + \frac{1}{2}\{w[x_0 - s(d_i), y_0, z_i] - w[x_0 + s(d_i), y_0, z_i]\} \cot\theta, \quad (2a)$$

$$\frac{b_4 - b_3}{2\sin\theta} = \frac{1}{2}\{v[x_0, y_0 - s(d_i), z_i] + v[x_0, y_0 + s(d_i), z_i]\} + \frac{1}{2}\{w[x_0, y_0 - s(d_i), z_i] - w[x_0, y_0 + s(d_i), z_i]\} \cot\theta, \quad (2b)$$

$$\frac{b_1 + b_2 + b_3 + b_4}{4\cos\theta} = \frac{1}{4}\{w[x_0 - s(d_i), y_0, z_i] + w[x_0 + s(d_i), y_0, z_i] + w[x_0, y_0 - s(d_i), z_i] + w[x_0, y_0 + s(d_i), z_i]\} + \frac{1}{4}\{u[x_0 - s(d_i), y_0, z_i] - u[x_0 + s(d_i), y_0, z_i] + v[x_0, y_0 - s(d_i), z_i] - v[x_0, y_0 + s(d_i), z_i]\} \tan\theta. \quad (2c)$$

If the horizontal dimensions of the feature (e.g., soliton or turbulence patch) are larger than the beam separation, then one can expand (2) in a Taylor series about x_0, y_0, z_i:

$$\frac{b_1 - b_2}{2\sin\theta} \equiv \tilde{u} \approx u(x_0, y_0, z_i) - \frac{\partial w}{\partial x} d_i + \frac{1}{2}\frac{\partial^2 u}{\partial x^2} d_i^2 \tan^2\theta + \cdots, \quad (3a)$$

$$\frac{b_4 - b_3}{2\sin\theta} \equiv \tilde{v} \approx v(x_0, y_0, z_i) - \frac{\partial w}{\partial y} d_i + \frac{1}{2}\frac{\partial^2 v}{\partial x^2} d_i^2 \tan^2\theta + \cdots, \quad (3b)$$

$$\frac{b_1 + b_2 + b_3 + b_4}{4\cos\theta} \equiv \tilde{w} \approx w(x_0, y_0, z_i) - \frac{1}{2}\left(\frac{\partial u}{\partial x} + \frac{\partial v}{\partial y}\right) d_i \tan^2\theta + \frac{1}{4}\left(\frac{\partial^2 w}{\partial x^2} + \frac{\partial^2 w}{\partial y^2}\right) d_i^2 \tan^2\theta + \cdots. \quad (3c)$$

The error consists of a term proportional to the distance from the transducer face times the horizontal shear of the perpendicular component at first order and the square of the distance times the second derivative of the normal component velocity at second order. If the horizontal gradients in the velocity field are small, corresponding to large spatial scales, only the zero-order terms are retained, and the transformations normally used to estimate ADCP mean velocities are obtained. Equations (3) represent the spatial convolution inherent in a single ADCP measurement. A temporal averaging may also be performed that further distorts a measurement of the true velocity field.

If the water is incompressible (a good assumption near the surface), then

$$\frac{\partial u}{\partial x} + \frac{\partial v}{\partial y} = -\frac{\partial w}{\partial z}. \quad (4)$$

Substitution into Eq. (3c) yields a first-order correction for w given by

$$\tilde{w} \approx \hat{w}(x_0, y_0, z_0) + \frac{1}{2}\left(\frac{\partial \hat{w}}{\partial z}\right) d_i \tan^2\theta, \quad (5)$$

where $\hat{w}$ is a corrected estimate of $\tilde{w}$. The correction is based on a first-order vertical derivative only, can be obtained readily from a single profile, and is independent of the horizontal orientation (azimuth) of the ADCP.

For turbulence studies, time scales are generally faster than the buoyancy period and the fluctuations are assumed to be advected by the mean flow (e.g., Marsden et al. 1993; McPhee 1994), the ''frozen turbulence'' hypothesis. Typically, the coordinate frame is rotated along the mean (20 min to hourly averaged) flow and the time derivatives are converted to spatial derivatives. Alternatively, for propagating features, the axes may be rotated along the phase velocity. The downstream spatial derivatives can be converted to time derivatives through

$$\frac{\partial w}{\partial t} = -(c + \overline{U})\frac{\partial w}{\partial x'}, \quad (6)$$

where c and $\overline{U}$ are the phase speed and mean advective velocities, respectively.

Two methods were considered for the implementation of the corrections. First, a numerical technique was used to invert Eq. (5). This method suffers from an incomplete specification of the initial boundary condition. For the second method, the vertical derivative was approximated from the raw data; that is,

$$\hat{w}(x_0, y_0, z_0) \approx \tilde{w} - \frac{1}{2}\left(\frac{\partial \tilde{w}}{\partial x}\right) d_i \tan^2\theta. \quad (7)$$

It was found that the two methods, except for the first bin, produced almost identical results and, given its ease of implementation, only (7) will be considered further. Corrections to the horizontal velocity were then made using the corrected vertical velocity as follows:

$$\hat{u}'(x_0, y_0, z_i) \approx \tilde{u}' - \frac{1}{c + \overline{U}}\frac{\partial \hat{w}}{\partial t} d_i, \quad (8)$$

where the primes indicate the frame rotated along the mean velocity. Note that the correction for the horizontal cross-stream velocity ($\tilde{v}'$) is assumed to be of second order. The absolute limit of ADCP resolution is, of course, governed by sampling theory. Features must have horizontal length scales greater that twice the bin size and separation to avoid aliasing.

3. Simulations

a. Internal waves

The first simulation mimics ensemble-averaging 100 pings in a 2-min ensemble from an ADCP with a 30° transducer angle. Modern pulse-to-pulse coherent ADCPs are quite accurate and for these system characteristics have errors of 0.173 cm s^{-1} for the vertical and 0.42 cm s^{-1} for the horizontal velocities, respectively. The rms error in the vertical gradient is given by

$$\sigma_d = \sqrt{2}\sigma_{\tilde{w}} d \tan^2(30°)/(2\Delta z), \quad (9)$$

and the overall error for the corrected vertical velocity is then

$$\sigma_{\hat{w}} = \sqrt{\sigma_{\tilde{w}}^2 + \sigma_d^2}. \quad (10)$$

Similarly, the error in the horizontal correction is given by

$$\sigma_t = \sqrt{2}\sigma_{\hat{w}} d/[(\overline{U} + c)\Delta t], \quad (11)$$

and the overall error is

$$\sigma_{\hat{u}} = \sqrt{\sigma_{\tilde{u}}^2 + \sigma_t^2}. \quad (12)$$

Averaging would typically be used for a long-term deployment with a low-frequency ADCP, such as that deployed by Schott and Leaman (1991) to detect vertical convection in the Gulf of Lyons or by Melling et al. (2001) for a long-term survey of the North Water Polynya. Here accuracy, data storage, and battery power considerations may necessitate ensemble averaging. The specific example will be internal solitary waves detected by Marsden et al. (1994b) in the Canadian Arctic. They show that the Benjamin (1966) model gives a crude, but fairly reasonable, estimate of some waves. It is a

shallow water, Boussinesq model for which the streamlines are given by

$$\psi = z + a\phi(z)\ \mathrm{sech}^2(\lambda x), \tag{13}$$

with horizontal and vertical velocities

$$v(x, \psi) = \frac{ac\phi'(z)\ \mathrm{sech}^2(\lambda x)}{1 + a\phi'(z)\ \mathrm{sech}^2(\lambda x)},$$

$$w(x, \psi) = \frac{2.0ac\lambda\phi(z)\ \sinh(\lambda x)\ \mathrm{sech}^3(\lambda x)}{1 + a\phi'(z)\ \mathrm{sech}^2(\lambda x)}, \tag{14}$$

where w and v are the vertical and horizontal velocities; a and c are the amplitude and phase speed, respectively, and are negative for waves of depression and waves traveling in the negative direction; and ϕ is the eigenvector and ϕ' its vertical derivative corresponding to the largest eigenvalue (c_0) of the Sturm–Liouville problem:

$$\frac{\partial}{\partial z}\left(c_0^2\rho\frac{\partial\phi}{\partial z}\right) - g\frac{\partial\rho}{\partial z}\phi = 0 \qquad \phi = 0;$$

$$z = 0, -h. \tag{15}$$

The phase speed (c) and length scale (λ) of the wave are given by

$$c^2 = c_0^2\left(1 + a\frac{\int_{-h}^{0}\rho\phi'^3\,dz}{\int_{-h}^{0}\rho\phi'^2\,dz}\right), \tag{16}$$

$$\lambda^2 a = 4\left(\frac{c^2\int_{-h}^{0}\rho\phi^2\,dz}{c_0^2\int_{-h}^{0}\rho\phi'^3\,dz}\right). \tag{17}$$

Profiles of the density, ϕ, and ϕ' were based on a cast taken at 1201 eastern standard time (EST) 30 April 1992 outside of Resolute, Nunavut, Canada. Details of the cast can be found in Marsden et al. (1994a). Care must be taken in implementing the model. The correction to the vertical velocity field [Eqs. (4) and (5)] is critically dependent on the incompressibility assumption. The model velocities were applied at the streamline depth, the results were differentiated numerically, and the incompressibility condition (critical for this method) was verified.

Equation (14) was then used to calculate a theoretical 15-m solitary wave that was then propagated in the $-x$ direction at the net speed of the wave ($c + \overline{U}$) = 40 cm s^{-1}, where c is the intrinsic phase speed from (14) and $\overline{U}$ is the background tidal flow. Normally, solitons are embedded in the mean flow. The time of the disturbance can be found from the vertical velocity. The background flow is then taken to be an average of the flow immediately preceding and following the flow disturbance. The model was then sampled and averaged at the appropriate depth-dependent separations (i.e., $\pm d_i \tan\theta$) as outlined in (2) to imitate the spatial convolution inherent in the measurement. These values were compared to an equivalently averaged ''direct'' wave (i.e., a simulated average of the depth cells at one point directly beneath the transducer face). The model horizontal and vertical velocities prior to convolution and averaging are shown in Figs. 2a and 2b. The maximum v is about 29 cm s^{-1} and is highly surface trapped within about 20 m of the ice–water interface, while the model predicts maximum vertical velocities of 7.7 cm s^{-1} at 63-m depth.

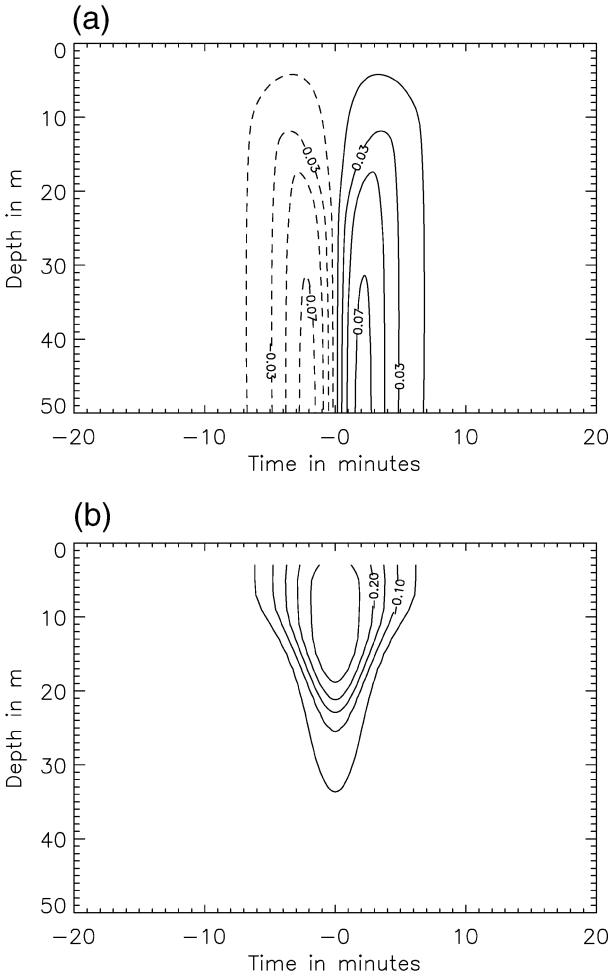

FIG. 2. Contour of simulated (a) vertical (w) and (b) anomaly horizontal (u) velocity fields. For (a) the dashed and solid lines represent downward and upward flows, and the contour interval is 0.02 m s^{-1}. In (b) the contour interval is 0.05 m s^{-1}.

The maximum absolute velocity differences between the direct and convolved wave were calculated to quantify the beam divergence problem. Alternatively, the rms errors could have been used, but these have the disadvantage of presenting an averaged view of the errors. The outer extremities of the disturbance will correspond

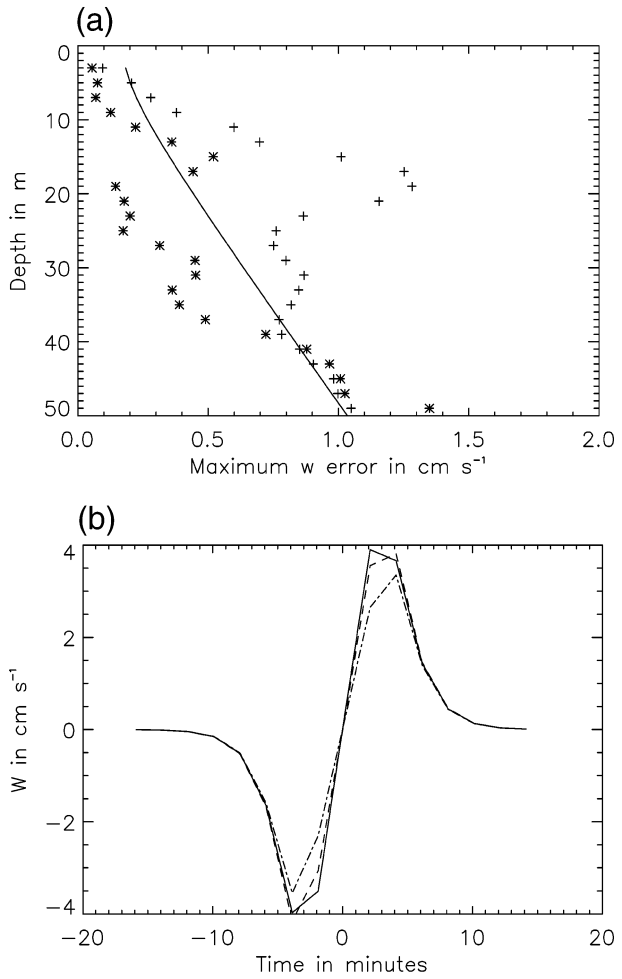

FIG. 3. (a) Maximum absolute error of the uncorrected (crosses) and corrected (stars) estimates of the vertical velocity as a function of depth. (b) The unconvolved (solid), convolved (dot–dashed), and corrected (dashed line) waves as a function of time at 17-m depth.

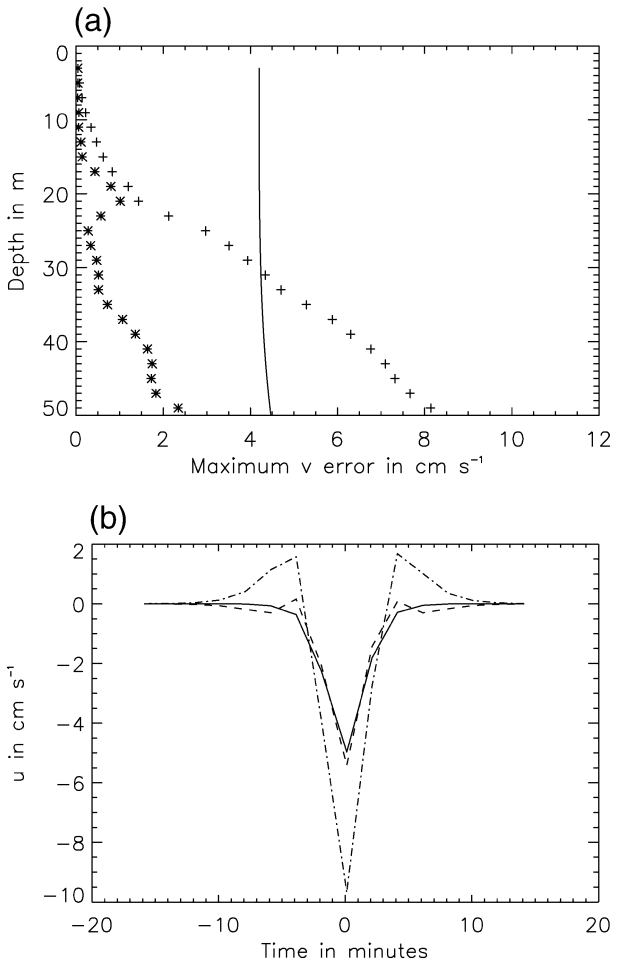

FIG. 4. Same as Fig. 3 for the horizontal velocity at 33-m depth.

to low velocities and hence present a conservative estimate. The maximum absolute error for the $\hat{w}$ (Fig. 3a) peaks at 17-m depth with a difference of about 1.3 cm s^{-1} (or about 20%) of the peak amplitude. The rms $\hat{w}$ errors as a function of depth using (9) and (10) are indicated by the solid line. The corrected amplitudes are below instrument noise levels to 40-m depth, below which the correction does not improve the estimate. Figure 3b shows the time series of the direct, or unconvolved (solid line), the convolved (dot–dashed line), and the corrected (dashed line) waves. The large discrepancies at the peaks are evident, as is the efficacy of the velocity correction. Figure 4a shows the expected maximum absolute error of the downstream velocity, u, as a function of depth. Here, a highly idealized correction was calculated using the 0.4 m s^{-1} phase speed ($c + U$) in (8). The uncorrected errors are less than 2 cm s^{-1} to 20 m from the transducer head and increase sharply below to more than 8 cm s^{-1} at 50-m depth. The solid line indicates expected instrument noise levels as determined from (11) and (12). The corrections are greater than the noise level below 30 m, and indeed errors in beam divergence dominate the signal. The correction reduces the maximum error throughout the water column and is less than the instrument noise level within 40 m of the transducer head. Figure 4b shows the true, convolved, and corrected velocities at 33-m depth. The error is quite profound and can be corrected to nearly match the wave profile. It must be noted, however, that the horizontal phase speed will probably never be known with absolute certainty from a single point measurement, and while the simulations demonstrate the potential gains in correcting the horizontal velocities, these may never be realizable.

b. Turbulence simulations

The previous results demonstrated the effects of beam divergence on internal solitary waves that have length scales that are relatively large compared with beam divergence. Several investigators (e.g., Stacey et al. 1999;

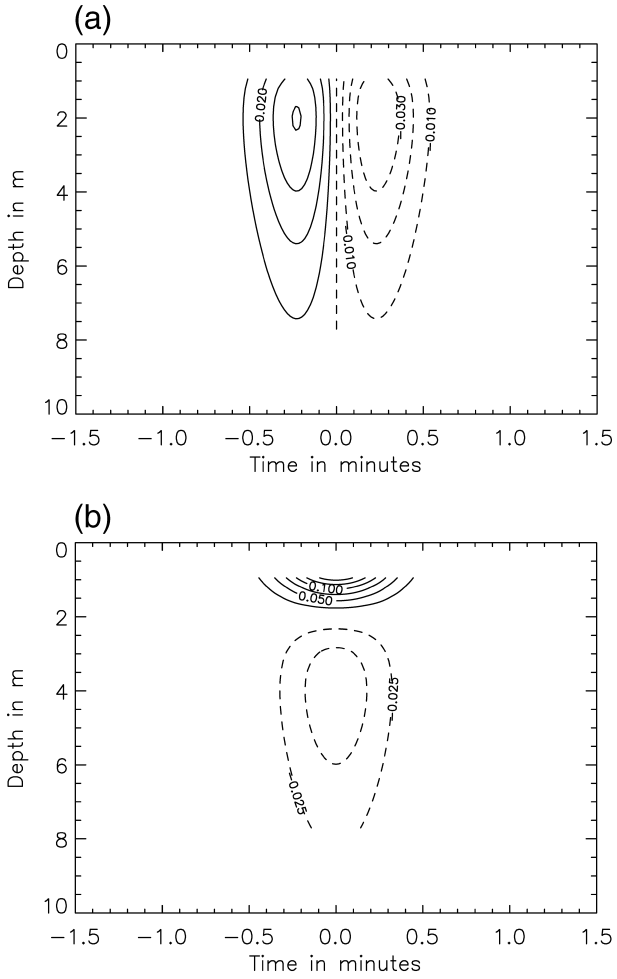

FIG. 5. Same as Fig. 2 for the simulated turbulence field. The contour intervals are 0.01 and 0.025 cm s^{-1} for the vertical and horizontal velocities, respectively.

Lu and Lueck 1999) have extended the use of the ADCP to turbulence scales. Here, the length scale of the flow would be of the same size as beam divergence, even very close to the transducer head. Marsden (2004, manuscript submitted to *J. Phys. Oceanogr.*) has investigated turbulence near the ice–water interface in the Canadian Arctic. He used a 614-kHz RDI ADCP set to pulse-to-pulse coherent mode (mode 11), sampling at 1.0 s in 28 depth cells at 0.25-cm increments. The instrument head was positioned 0.54 m below the ice–water interface yielding the first sampling bin at 0.94 m. This mode was very accurate as sampling during quiescent periods indicated rms errors of 0.15 and 1.2 cm s^{-1} per ping in the vertical and horizontal velocities, respectively. The increased resolution and accuracy came at the cost of penetration, as results could only be obtained within 8 m of the transducer head. The minimum horizontal resolvable length scales, that are not aliased, range from 0.5 m in bin 1, due to the 0.25-m bin size, to 10.2 m at 7 m from the transducer head, due to beam divergence.

Simulations suggest that beam divergence is a problem and can be rectified in the vertical and longitudinal velocities. For turbulence studies, normally (McPhee 1994) the mean flow is determined over, say, a 1-h period, and turbulence parameters are calculated from the deviatory velocities. The form of the streamfunction for modeling turbulent fluctuations was taken to be

$$\psi(x, z) = az \exp\left[-\left(\frac{z}{b} + \frac{1}{2}\frac{x^2}{c^2}\right)\right] \Big/ b. \qquad (18)$$

The horizontal ($u = -\partial\psi/\partial z$) and vertical ($w = \partial\psi/d\partial x$) velocities were calculated for a number of estimates of b, c, and background flows ($\overline{U}$). The values of b and $2.0 \times c$ represent the length scales of the vertical and horizontal velocities, respectively. This form forces the vertical velocity fluctuation to be 0.0 at the wall. The amplitude a was adjusted to give typical velocities found in the data. In all cases, beam divergence was significant for the horizontal velocities and estimates could be improved. Figures 5a and 5b show the vertical and horizontal velocities associated with typical values of $b = 2.0$, $c = 5.5$, and $\overline{U} = 40$ cm s^{-1}. The vertical velocity field is a doublet with maximum values of 3.0 cm s^{-1}, while the horizontal velocity is surface trapped with a maximum value of about 17.0 cm s^{-1}. The simulations were found to be insensitive to the advection speed $\overline{U}$. A large value is preferable, however, to dominate any possible intrinsic phase speed of the eddies and to reduce the correction error of (11). Since the time scale of the fluctuations is greater than the minimum buoyancy period of the water column, the influence of internal waves should be small.

Figure 6a shows that maximum error in the vertical velocity is very small (<1.5 mm s^{-1}), considerably less than the instrument noise level. Figure 6b indicates the direct (solid line), measured (dot–dashed line), and corrected (dashed line) values for the 14th bin, 4.0 m from the transducer face. The errors are small and the correction only marginally improves the results near the transducer head. Figure 7a shows the maximum absolute error of the horizontal velocity as a function of depth. Maximum values of the uncorrected velocities are 2.0 cm s^{-1}, above the instrument noise level, between 1.5- and 6.0-m depth, indicated by the solid line. Figure 7b shows the actual, measured, and corrected values at 4.0-m depth. The extent of the beam divergence error and its subsequent correction are quite striking. The simulations were run for considerable ranges in values for b and c, and the results were similar. Errors in the vertical velocity were negligible, while corrections to the horizontal longitudinal velocities were quite profound and brought maximum errors below the instrument noise level.

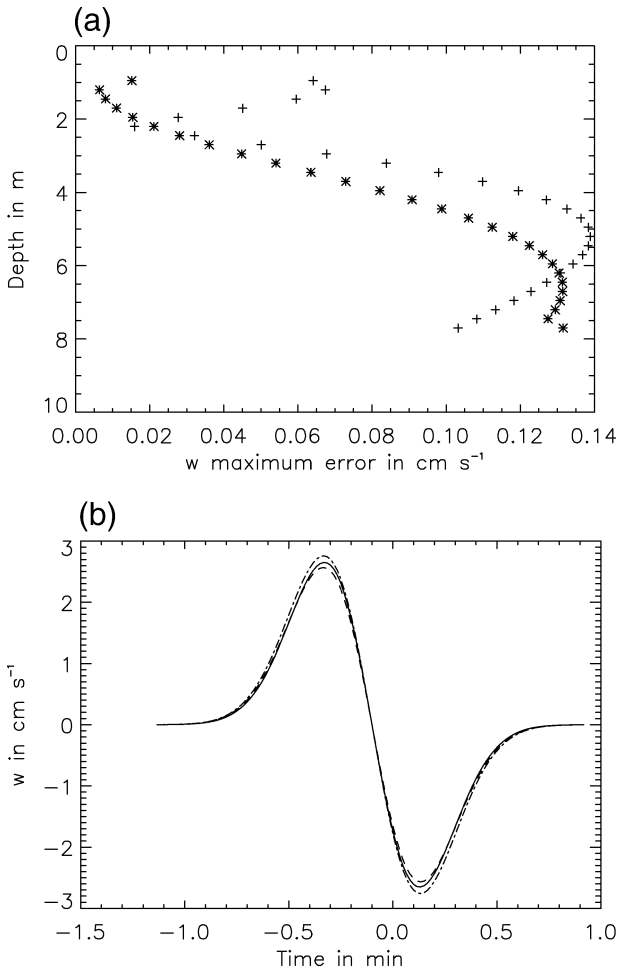

FIG. 6. Same as Fig. 3 for the vertical velocities of the simulated turbulent velocity field. The sample field is at 7.7-m depth.

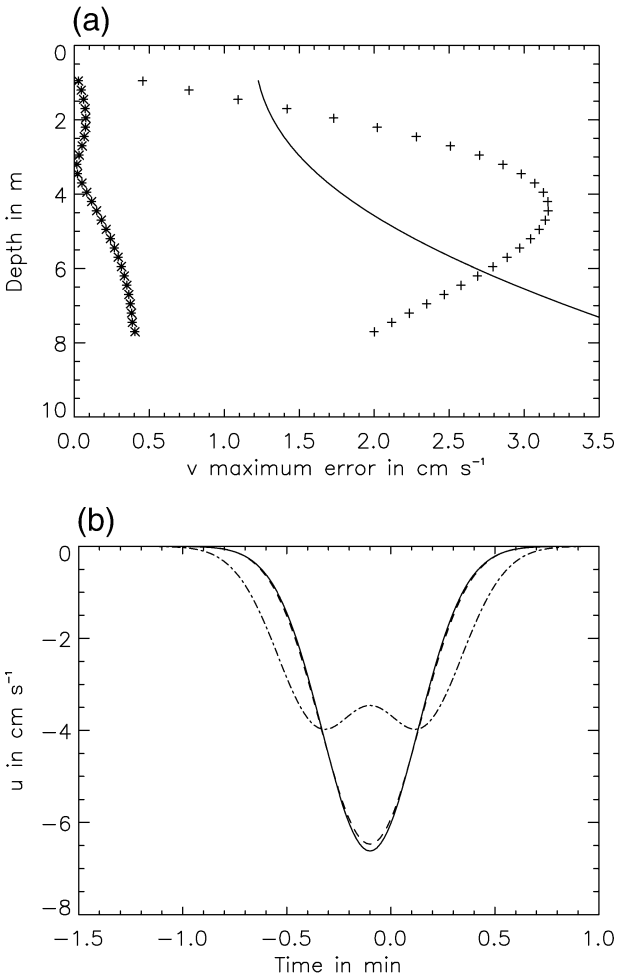

FIG. 7. Same as Fig. 4 for the horizontal velocities of the simulated turbulent velocity field. The sample field is at 7.7-m depth.

4. Conclusions

The objective of this paper is to investigate the effect of beam divergence on ADCP velocity estimates. An analysis of beam separation and application of incompressibility lead to a proposed correction to account for beam divergence in the vertical velocity. Assuming that features were advected by the wave or the mean flow allowed for correction of the longitudinal horizontal velocities. These ideas were initially tested for a 30° transducer angle with 100 ensembles averaged over 120 s. The correction improved the simulation results to within about 40 m from the transducer head, after which it was ineffective. Within 20 m of the transducer head the corrected estimate showed rms errors to be about one-third of the uncorrected values. Application of the correction to the sampled data indicated much larger vertical velocities with depth, as suggested by the model. While perhaps only a theoretical exercise, the corrections to the horizontal velocities for the soliton case were quite striking. Turbulent eddies were also modeled. In general, errors in the vertical velocity to the 8-m penetration depth of the ADCP were very small. The horizontal velocity errors were much larger and could be corrected to below instrument noise level. Furthermore, the frozen turbulence hypothesis is expected to hold in cases of high background flow, as presented by Stacey et al. (1999) and Lu and Lueck (1999). Finally, all errors were a maximum at maximum flow amplitude, precisely when accurate estimates are required. It could be argued that the results simulate older ADCP designs and are no longer applicable. However, these results are independent of manufacturer or specific instrument, being dependent only on beam geometry. The ADCP models cited here define instrument noise level, and the advent of newer, more accurate ADCPs only strengthens the argument for application of these corrections.

The significance of the correction could have profound consequences. First, high-frequency internal waves and solitons are characterized by fluctuations in the vertical velocity field. It is absolutely critical that these be identified and accurately measured. It is quite clear that the ADCP can accurately record the vertical

velocity to within several millimeters per second and the horizontal velocity to within several centimeters per second within 30 m of the transducer head. Second, McPhee (1994) shows that friction velocity and turbulent dissipation can be measured from vertical velocities alone using the ''inertial dissipation'' method. He further states (p. 2019) that ''high-resolution acoustic Doppler current profilers, for example, may soon provide more-or-less continuous vertical velocity data through most of the mixed layer.'' Finally, it must be noted that these results are equally applicable to upward-looking ADCPs rigidly mounted on the ocean floor. In this configuration, further corrections may be required to account for possible misalignment with the vertical.

Acknowledgments. RFM and RGI were funded by the Canada–Japan Science and Technology Fund through the Department of External Affairs, Canada. RFM received additional funding from the academic research program of the Department of National Defence of Canada. RGI received additional funding from NSERC and Fonds FCAR of Quebec. Two anonymous reviewers provided particularly insightful comments that greatly improved the final version of the manuscript.

REFERENCES

Benjamin, T. B., 1966: Internal waves of finite amplitude and permanent form. *J. Fluid Mech.*, **25,** 241–270.

Foreman, M. G. G., and H. J. Freeland, 1991: A comparison of techniques for tide removal from ship-mounted acoustic Doppler measurements along the southwest coast of Vancouver Island. *J. Geophys. Res.*, **96,** 17 007–17 021.

Lohrmann, A., B. Hackett, and L. P. Roed, 1990: High resolution measurements of turbulence velocity and stress using a pulse-to-pulse coherent sonar. *J. Atmos. Oceanic Technol.*, **7,** 19–37.

Lu, Y., and R. G. Lueck, 1999: Using a broadband ADCP in a tidal channel. Part I: Mean flow and shear. *J. Atmos. Oceanic Technol.*, **16,** 1556–1567.

——, and K. C. Greenwood, 1994: Internal tides observed by an acoustic Doppler current profiler. *J. Phys. Oceanogr.*, **24,** 1097–1109.

——, G. A. McBean, and B. A. Proctor, 1993: Momentum and sensible heat fluxes calculated by the dissipation technique during the Ocean Storms project. *Bound.-Layer Meteor.*, **63,** 23–38.

——, R. G. Ingram, and L. Legendre, 1994a: Currents under land-fast ice in the Canadian Arctic Archipelago. Part 2: Vertical mixing. *J. Mar. Res.*, **51,** 1037–1049.

——, R. Paquet, and R. G. Ingram, 1994b: Currents under land-fast ice in the Canadian Arctic Archipelago. Part 1: Vertical velocities. *J. Mar. Res.*, **51,** 1017–1036.

——, B.-A. Juszko, and R. G. Ingram, 1995: Internal wave directional spectra using an acoustic Doppler current profiler. *J. Geophys. Res.*, **100,** 16 179–16 192.

McPhee, M. G., 1994: On the mixing length in the oceanic boundary layer. *J. Phys. Oceangr.*, **24,** 2014–2031.

Melling, H., Y. Gratton, and G. Ingram, 2001: Ocean circulation within the North Water Polynya of Baffin Bay. *Atmos.-Ocean*, **39,** 301–325.

RDI, 1996: *Acoustic Doppler Current Profiler: Principles of Operation—A Practical Primer*. RD Instruments, Inc., 54 pp.

Schott, F., and K. D. Leaman, 1991: Observations with moored acoustic Doppler current profilers in the convection regime in the Golfe du Lion. *J. Phys. Oceanogr.*, **21,** 558–574.

Stacey, M. T., S. G. Monismith, and J. R. Burau, 1999: Observations of turbulence in a partially stratified estuary. *J. Phys. Oceanogr.*, **29,** 1950–1970.

van Haren, H., N. Oakey, and C. Garrett, 1994: Measurements of internal wave band eddy fluxes above a sloping bottom. *J. Mar. Res.*, **52,** 909–946.